Volume 9 | Number 1 | January 2016 | Pages 1–268

Energy & Environmental Science

www.rsc.org/ees

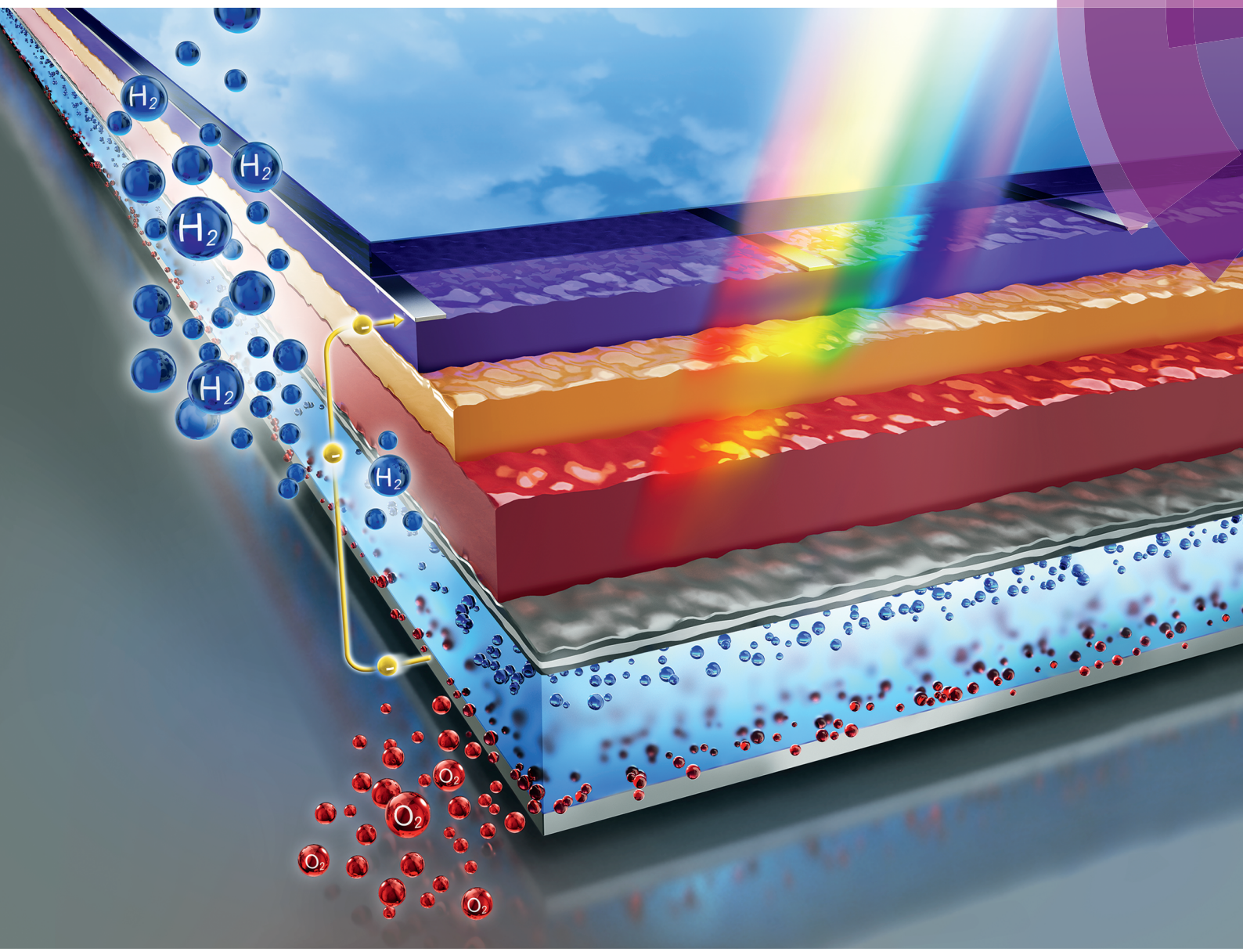

ISSN 1754-5692

ROYAL SOCIETY OF CHEMISTRY

PAPER
Félix Urbain *et al.*
Multijunction Si photocathodes with tunable photovoltages from 2.0 V to 2.8 V for light induced water splitting

175 YEARS

Energy & Environmental Science

PAPER

View Article Online
View Journal | View Issue

Cite this: *Energy Environ. Sci.*, 2016, **9**, 145

Multijunction Si photocathodes with tunable photovoltages from 2.0 V to 2.8 V for light induced water splitting†

Félix Urbain,*[a] Vladimir Smirnov,[a] Jan-Philipp Becker,[a] Andreas Lambertz,[a] Florent Yang,[b] Jürgen Ziegler,[b] Bernhard Kaiser,[b] Wolfram Jaegermann,[b] Uwe Rau[a] and Friedhelm Finger[a]

Received 4th August 2015,
Accepted 5th October 2015

DOI: 10.1039/c5ee02393a

www.rsc.org/ees

We report on the development of high performance triple and quadruple junction solar cells made of amorphous (a-Si:H) and microcrystalline silicon (μc-Si:H) for the application as photocathodes in integrated photovoltaic–electrosynthetic devices for solar water splitting. We show that the electronic properties of the individual sub cells can be adjusted such that the photovoltages of multijunction devices cover a wide range of photovoltages from 2.0 V up to 2.8 V with photovoltaic efficiencies of 13.6% for triple and 13.2% for quadruple cells. The ability to provide self-contained solar water splitting is demonstrated in a PV-biased electrosynthetic (PV-EC) cell. With the developed triple junction photocathode in the a-Si:H/a-Si:H/μc-Si:H configuration we achieved an operation photocurrent density of 7.7 mA cm^{-2} at 0 V applied bias using a Ag/Pt layer stack as photocathode/electrolyte contact and ruthenium oxide as counter electrode. Assuming a faradaic efficiency of 100%, this corresponds to a solar-to-hydrogen efficiency of 9.5%. The quadruple junction device provides enough excess voltage to substitute precious metal catalyst, such as Pt by more earth-abundant materials, such as Ni without impairing the solar-to-hydrogen efficiency.

Broader context

Solar-driven water splitting, a process that mimics natural photosynthesis, provides a viable example of an ecofriendly energy concept as it converts solar energy into a storable and clean chemical fuel, namely hydrogen. To be competitive with fossil fuels or hydrogen production by other means, this process must however become highly efficient and low-cost. Integrated semiconductor based photoelectrochemical systems emerged as adequate candidates and have been attracting considerable interest among research groups worldwide. In the scientific literature, numerous studies have successfully demonstrated unbiased solar water splitting using Si based photovoltaic-electrochemical (PV-EC) devices. To maximize the solar-to-hydrogen efficiency, the photovoltaic cells, however, need to be specifically designed to match electrical parameters for water splitting. Therefore, the present study focuses on the tuning of both, the electrochemical and the photovoltaic parameters of integrated Si based PV-EC devices with respect to the water splitting requirements. We demonstrate the applicability of various types of multijunction photocathodes in PV-EC device configuration which provide a wide range of adjustable photovoltages from 2.0 to 2.8 V. Thereby, the variety of feasible applications and material combinations in photoelectrochemical systems is considerably extended, leading to a remarkable solar-to-hydrogen efficiency of 9.5%.

I. Introduction

Efficient production of clean and storable chemical fuels, such as hydrogen, from solar energy is of utmost importance for future sustainable post-carbon energy systems.[1,2] It is therefore vital to develop and improve efficient artificial processes to convert the energy of light into chemical energy. For this purpose, photoelectrolysis of water by semiconductor based devices represents a prominent route which recently raised increasing interest among research groups worldwide.[3–5] Photoelectrolysis of water is a chemical process that produces hydrogen (and oxygen) and requires light induced potential differences, *i.e.* photovoltages over 1.6 V to run autonomously, taking into account the overpotential losses in such systems.[6] Among state-of-the-art solar fuel generators, photovoltaic (PV)-biased electrosynthetic cells (denoted as PV-EC devices hereafter), which consist of a solar cell, submerged in an electrolyte and electrically arranged in

[a] *IEK-5 Photovoltaik, Forschungszentrum Jülich, D-52425, Jülich, Germany. E-mail: f.urbain@fz-juelich.de*
[b] *Institute of Materials Science, TU Darmstadt, D-64287, Darmstadt, Germany*

† Electronic supplementary information (ESI) available. See DOI: 10.1039/c5ee02393a

series with electrocatalysts for the hydrogen (HER) and oxygen evolution reaction (OER), respectively, offer several advantages compared to other photoelectrochemical device configurations:[7]

- In a PV-EC device the photovoltage and the photocurrent generated by the underlying solar cell are entirely available for the photoelectrolysis, *i.e.* the solar cell can be adjusted independent from any electrochemical reaction at the solar cell/electrolyte interface[8,9] or any second photoactive electrode material.[10]
- Such flexibility, so far, allowed for higher achievable efficiencies compared to other solar fuel generator configurations.[11]
- The current–voltage characteristics of the electrocatalysts can be merged with the PV characteristics of the solar cell, in terms of a simple series connection, to accurately predict the PV-EC device performance.[12–14]

Among the semiconductor technologies used for solar water splitting, multijunction thin film silicon solar cell structures have been explored for over 20 years now and have acquired a leading position,[10,15–19] thanks to their ability to provide high photovoltages in multijunction structures above the required potential for photoelectrolysis.[9] The highest reported solar-to-hydrogen (STH) efficiencies for monolithic thin film silicon based solar fuel generators are 6.8% for tandem[12] and 7.5% and 7.8%, respectively, for triple junction based photoelectrodes made of hydrogenated amorphous silicon (a-Si:H).[19,20] The thin film silicon device concept allows to fabricate monolithic cells, which can be integrated in a compact water splitting device. Other studies, in contrast, use module connections of several solar cells, *e.g.* III–V based, CIGS, crystalline silicon, or perovskite solar cells,[21–24] to provide the sufficient voltage to run the HER and OER, respectively, without an external bias. Although, the achieved STH efficiencies in module based water splitting devices are remarkable,[11] the multijunction thin film silicon concept offers several advantages compared to series connected solar cells: in general the series connection requires an additional processing step (laser scribing or solar tabbing wire connection) compared to the monolithic multijunction solar cell fabrication process, which becomes particularly relevant in industrial applications. Additionally, series connected cells cannot be adjusted precisely with respect to the specifically needed photovoltage of the complete system, which varies with the overpotentials of the used catalysts for the HER and OER, respectively. Considering that the photocurrent at the respective required voltage determines the STH efficiency,[6] the photovoltage/photocurrent tradeoff, prevented higher STH efficiencies so far. In crystalline silicon solar cells, for instance, the photovoltage can be adjusted only in large steps of approx. 600 mV by connecting several cells in series. However, in such case the increase in voltage is accompanied by a significant decrease in photocurrent and device efficiency (if the active solar cell area remains unchanged). The same however also applies to multijunction solar cells made merely of amorphous silicon alloys (a-Si:H and a-Si:Ge:H), which have been applied for unbiased solar water splitting by Delahoy *et al.* and Khaselev *et al.* for instance.[15,20] Therefore, it is crucial to develop solar cells with the ability to tune the photovoltage not only in large but also in small steps in order to fulfill the particular requirements of various PV-EC systems. At the same time a change in the photovoltage should ideally not impair the device efficiency.

This task can be performed by monolithic multijunction solar cells made of thin films of amorphous (a-Si:H) and microcrystalline (μc-Si:H) silicon, which were developed in this study. Combinations of a-Si:H and μc-Si:H allow for a more precise adjustment of the PV parameters and suffer less from stability issues under prolonged illumination (Staebler–Wronski effect)[25] compared to their all-amorphous counterparts.[26] In fact, the present study builds on a previous work,[12] in which the fundamental working principle of a a-Si:H/a-Si:H tandem based PV-EC device has been demonstrated and validated by empirical modeling. In the present work now, we developed a-Si:H/μc-Si:H/μc-Si:H and a-Si:H/a-Si:H/μc-Si:H triple and a-Si:H/a-Si:H/μc-Si:H/μc-Si:H quadruple junction solar cells aiming to provide higher STH efficiencies in PV-EC configuration and higher tunable excess voltages to have a higher flexibility in choosing different catalyst materials with different overpotential requirements. Extending beyond former studies on thin film silicon multijunction photoelectrodes,[10,15–17] the present work demonstrates the tunability of voltages over a very wide range. Thereby, the variety of feasible applications in photoelectrochemical systems is considerably extended. We used a-Si:H sub cells with different optical band gaps, as well as μc-Si:H absorber layers with improved stability against light-induced degradation which leads to an improved solar cell performance. Particularly, the photocurrent density was significantly improved (by 0.8 mA cm^{-2}) by implementing microcrystalline silicon oxide (μc-SiO_x:H) as intermediate reflecting layers[27] and by carefully adapting the thicknesses of the individual sub cells. The applicability of the developed solar cells as photocathodes in an integrated PV-EC device is further demonstrated with thin Pt and Ni catalyst layers, respectively on top of the solar cells for the HER and a RuO_2 counter electrode for the OER. Additionally, the associated aspects of the PV-EC device performance were addressed. In particular, the long-term durability as required for commercial applications has already been emphasized previously.[28–31] Besides the electrochemical stability, the present study furthermore investigates the aspects of catalysis and electrolyte dependence on the performance of the developed multijunction Si photocathodes.

II. Experimental details

A. Preparation of thin film silicon layers and solar cells

All thin film silicon layers were deposited by a plasma enhanced chemical vapor deposition technique in a multi chamber system. For the intrinsic absorber layers a mixture of silane (SiH_4) and hydrogen (H_2) gases was used. For the n- and p-type layers, trimethylborane (TMB), methane (CH_4), phosphine (PH_3), and carbon dioxide (CO_2) gases were added to the silane–hydrogen mixture. For μc-Si:H intrinsic and p-type layer depositions an excitation frequency of 94.7 MHz was applied. For all a-Si:H layers an excitation frequency of 13.56 MHz was applied. The triple and quadruple junction solar cells were made in stacked p–i–n superstrate configuration with a sputtered zinc oxide/silver

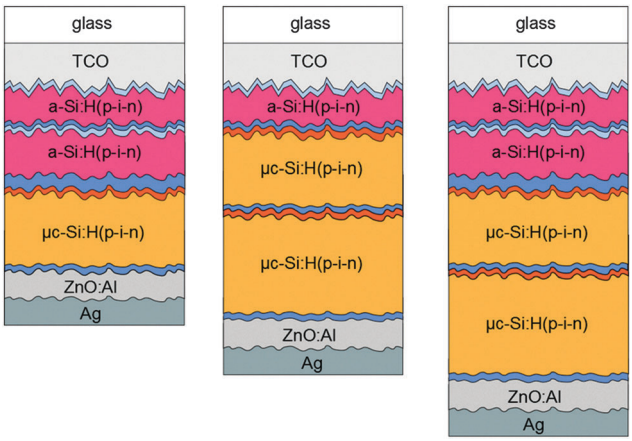

Fig. 1 Schematic drawing of the a-Si:H/a-Si:H/μc-Si:H and a-Si:H/μc-Si:H/μc-Si:H triple and a-Si:H/a-Si:H/μc-Si:H/μc-Si:H quadruple junction solar cell structures in p–i–n configuration investigated in this study.

(ZnO:Al/Ag) reflecting rear contact[32] defining the area (1 cm^2) of the individual cells. For all intrinsic μc-Si:H absorber layers a silane concentration (SC) of 5.0%, defined as the ratio between the SiH_4 flow and the total gas flow, and a substrate deposition temperature (T_S) of 180 °C was chosen.[26] The intrinsic a-Si:H top and middle cell absorber layers were deposited at 130 °C with a SC of 4% and at 180 °C with a SC of 10%, respectively.[9] The p- and n-type layers are the same for all fabricated solar cells and are deposited at a T_S of 180 °C. The a-Si:H/a-Si:H/μc-Si:H triple cells were deposited on 100 cm^2 fluorine-doped tin dioxide (SnO_2:F) coated glass substrates (front contact) with a native texture (Asahi U). The a-Si:H/μc-Si:H/μc-Si:H and quadruple cells were deposited on 100 cm^2 textured aluminum-doped ZnO coated glass substrates (front contact). Fig. 1 schematically shows the multijunction solar cell configurations investigated in this study.

Characterization of solar cells. The solar cells were characterized by current–voltage (J–V) measurements at standard test conditions (100 mW cm^{-2}, 25 °C) using a double source (Class A) AM 1.5 sun simulator with an anti-reflection foil on top of the front glass.[33] Furthermore, spectral response measurements [quantum efficiency (QE)] of the multijunction solar cells were conducted using a monochromator in a wavelength range between 300 nm to 1100 nm. Individual sub cell QEs of the triple and quadruple cells were separately determined using LEDs and a spectrally filtered bias light from a tungsten lamp. Bias light intensities of approximately 1 mW cm^{-2} were used to saturate the respective sub cells, while the intensity of the probing light was around 1000 times lower. The corresponding wavelengths used for the saturation of the sub cells are presented in Table 1.

As an example, for the a-Si:H/μc-Si:H/μc-Si:H triple cell, light with 695 nm wavelength was used for the saturation of the middle and bottom cell assuring that the top cell, which photocurrent is intended to be measured, limits the current of the whole device. For the measurement of the bottom cell, light of 525 nm wavelength was used to saturate the top and the middle cell. In the case of the middle cell QE measurement, the top cell is saturated with a 470 nm light and the bottom cell is saturated with 765 nm light.

B. Photoelectrochemical measurements

The integrated PV-EC device is schematically depicted as band diagram illustration in Fig. 2. It is composed of four main components: the multijunction solar cell (p–i–n type photocathode) to provide sufficient photovoltage and photocurrent for the water splitting reactions, a catalyst layer to enhance the HER, which is deposited on top of the solar cell at the photocathode/electrolyte interface, the electrolyte, which should provide high ionic conductivity, and an anode, coated with a catalyst to enhance the OER. The photoelectrochemical performance of the PV-EC devices was evaluated at room temperature in aqueous 0.1 M and 1 M KOH solutions using a two-electrode configuration.[34] The HER catalyst layer (Pt and Ni in this study) was deposited by electron beam evaporation with a thickness of around 150 nm on top of the Ag contact pads of the solar cell. In fact, the solar cell together with the attached HER catalyst compose the photocathode of the PV-EC device. The photocathode–electrolyte contact area was defined by an O-ring sealing aperture and was 0.5 cm^2. For the OER catalyst, a RuO_2 coated titanium sheet was used as anode (15 g m^{-2} RuO_2, 3 cm^2 active area, supplied by Metakem). Photocathode and anode were separated by a distance of 2 cm. White light photocurrent measurements were performed under simulated AM 1.5 solar illumination (100 mW cm^{-2}) using an Oriel LCS-100 solar simulator (model 94011A) and an optical aperture of 0.5 cm^2. Linear sweep voltammetry measurements were performed with a scan rate of 30 mV s^{-1} without stirring of the electrolyte. Electrical contact to the transparent conductive oxide (TCO) coated glass substrate, *i.e.* the front contact of the solar cell, was made by a silver paste. The PV-EC devices were illuminated through the glass substrate of the integrated solar cell (see Fig. 2), which offers the advantage that the light enters the photocathode through the TCO coated glass substrate without being attenuated by a surrounding

Table 1 Overview of the used light wavelengths for the saturation of the individual sub cells in triple and quadruple junction solar cells for the QE evaluation

	Measured sub cell			
Cell type	Top cell	Middle cell 1	Middle cell 2	Bottom cell
a-Si:H/μc-Si:H/μc-Si:H	695 nm	765 nm and 470 nm	—	525 nm
a-Si:H/a-Si:H/μc-Si:H	590 nm	780 nm and 400 nm	—	525 nm
a-Si:H/a-Si:H/μc-Si:H/μc-Si:H	590 nm	780 nm and 400 nm	525 nm and 830 nm	625 nm

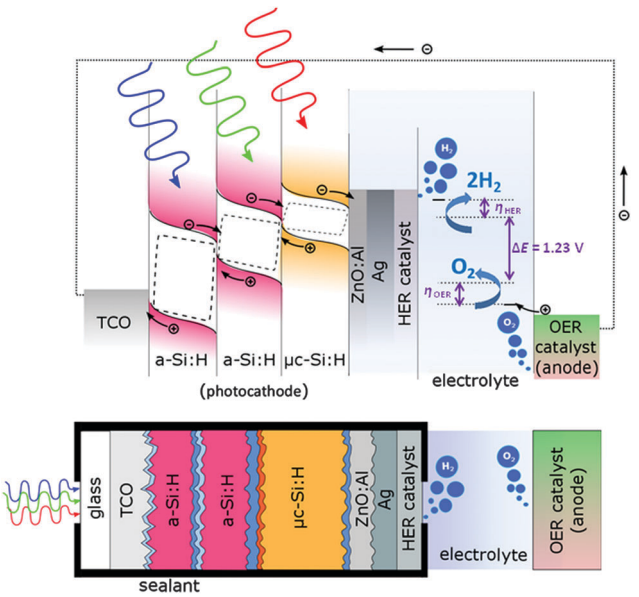

Fig. 2 Band diagram illustration of the PV-EC device configuration investigated in this study, with its components: the multijunction photocathode (as example a-Si:H/a-Si:H/μc-Si:H) under non-biased illumination condition, a HER catalyst layer at the photocathode/electrolyte interface, the electrolyte, and the anode with the OER catalyst. The energy levels for the HER and OER and the respective reactions are indicated in the illustration. Hydrogen evolution occurs at the rear side of the photocathode and oxygen evolves at the anode side. ΔE = 1.23 V is the thermodynamic potential required for water electrolysis at 25 °C. η_{HER} and η_{OER} indicate the overpotentials for the HER and OER, respectively.

medium (*e.g.* the electrolyte or gas bubbles). A major role in this configuration is governed by the metallic contact at the photocathode/electrolyte interface, which has to fulfill multiple requirements: (i) optical reflection of incident light back into the photocathode, (ii) protection of the photocathode from the electrolyte and undesired chemical reactions, and (iii) promotion of the catalytic reaction and a good electrical contact between the photocathode and the electrolyte. In this regard, a contact stack of ZnO:Al, Ag, and HER metal catalyst was used. The ZnO:Al/Ag double layer was used to ensure a good reflectivity of the incoming light, and thus allow for a high photocurrent. The thin metal layer deposited on top of the Ag layer was used as a catalyst for the HER.[9,12,26]

Nevertheless, for industrial applications a two-compartment set-up for the OER and HER, respectively separated through a membrane for quantitative gas amount evaluation is desirable and currently under construction. The configuration used in this study particularly aims to test prototype PV-EC devices based on our developed solar cells.

III. Results and discussion

A. Multijunction solar cells

The development of individual sub cells (a-Si:H and μc-Si:H single junction solar cells) of a multijunction device has been addressed in detail elsewhere.[9,26] The present study investigates the combination in triple and quadruple junction solar cells and exploits ways to improve the device efficiency in combination with high V_{OC} ranging from 2.0 V to 2.8 V. Due to requirements on the band gap sequence, the top and bottom cell absorber layers were made of a-Si:H (high band gap) and μc-Si:H, respectively, for all investigated multijunctions. For the middle cell absorber layers in triple junction solar cells either a-Si:H (lower band gap) or μc-Si:H were applied, which leads to different voltage and current matching conditions and represents the two development paths discussed below.

A1. a-Si:H/μc-Si:H/μc-Si:H triple junction solar cells. A target for a-Si:H/μc-Si:H/μc-Si:H triple junction solar cells was to achieve higher V_{OC} values than state-of-the-art a-Si:H/a-Si:H tandem junctions, *i.e.* above 1.9 V. Additional emphasis was put on photocurrent-matching of the individual sub cells and an increase in J_{SC} by integrating n-type μc-SiO_x:H layers.[27,35,36] For the top cell absorber layer a high band gap a-Si:H material (1.95 eV ± 25 meV) was chosen to increase the light incoupling and the V_{OC}.[9] Furthermore, the V_{OC} was increased by integrating nominally identical thin intrinsic a-Si:H buffer layers at the i–n interface of the μc-Si:H sub cells. Similar approaches were previously described for μc-Si:H single junction solar cells.[26,37] To evaluate the different routes, we investigated four different types of a-Si:H/μc-Si:H/μc-Si:H cells (referred to as T1–T4):

- a reference solar cell fabricated without μc-SiO_x:H layers and without n–i buffer layer (“T1”),
- a cell with μc-SiO_x:H layers for middle (⟨n2⟩) and bottom cell (⟨n3⟩) without n–i buffer layer (“T2”),
- the same cell as T2, but with 30 nm n–i buffer layer for the bottom cell (“T3”),
- the same cell as T2 with a 30 nm buffer layers for the bottom and a 20 nm thin buffer layer for the middle cell (“T4”).

Table 2 summarizes the performance of these triple junction cells, including layer preparation and PV parameters of the solar cells.

The sub cells had a thickness of 160 nm for the top, 1200 nm for the middle, and 1600 nm for the bottom cell. As presented in Table 2, the integration of μc-SiO_x:H as intermediate reflecting layers effectively increased the photocurrent density by 0.4 mA cm^{-2} (T1 to T4). Through the integration of intrinsic a-Si:H buffer layers at the μc-Si:H n–i interfaces the V_{OC} was increased by around 60 mV for one buffer layer (T3) and around

Table 2 Overview of all relevant layer preparation and PV parameters (V_{OC}, J_{SC}, FF, and efficiency η) of a-Si:H/μc-Si:H/μc-Si:H devices

Cell no.	μc-SiO_x:H ⟨n2⟩ and ⟨n3⟩ layers	n–i buffer layer	V_{OC} [mV]	J_{SC} [mA cm^{-2}]	FF [%]	V_{MPP} [mV]	J_{MPP} [mA cm^{-2}]	η [%]
T1	W/o	W/o	1906	8.0	69.6	1598	6.6	10.6
T2	With	W/o	1895	8.3	70.8	1602	6.8	11.1
T3	With	Bottom	1958	8.3	68.1	1596	6.9	11.1
T4	With	Bottom and middle	1976	8.4	67.6	1590	7.1	11.2

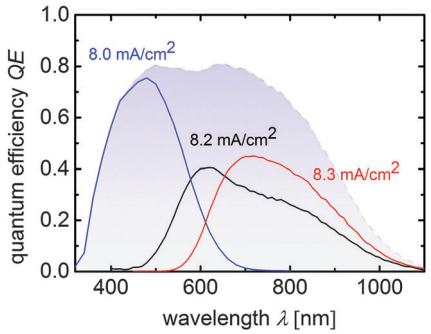

Fig. 3 Quantum efficiency curves of a a-Si:H/μc-Si:H/μc-Si:H triple junction device corresponding to cell T4 from Table 2. Sub cell current densities calculated from the QE-curves are placed near the related measurements and the total QE is displayed by the blue shaded area.

80 mV to 1976 mV for two buffer layers for middle and bottom cell (T4), along with a slight decrease in FF. Although the voltage at MPP was around 1.6 V for all cells, the current at MPP was increased by approx. 0.5 mA cm^{-2} from cell T1 to T4. Overall this result exemplarily demonstrates that the V_{OC} can be tuned very systematically within a small voltage range, while the photocurrent at the MPP of the solar cell can be adjusted without impairing the device efficiency. This is relevant in particular for water splitting applications, as it allows to precisely adjust the PV parameters to the overpotential requirements of different catalyst materials.

Fig. 3 depicts the quantum efficiency measurement of the triple junction cell T4. The QE shows that all sub cells have very similar photocurrent densities of 8.0 mA cm^{-2}, 8.2 mA cm^{-2}, and 8.3 mA cm^{-2} as presented in Fig. 3.

These values are slightly lower than the J_{SC} value quoted in Table 2, where an anti-reflection foil was additionally used during *J–V* measurements. From the total QE photocurrent (shaded in blue) a slight dip between 500 nm and 650 nm is visible, which corresponds to reflection losses at the intermediate reflecting/absorber layer interface.

A2. a-Si:H/a-Si:H/μc-Si:H triple junction solar cells. With the a-Si:H/a-Si:H/μc-Si:H triple junction cells the V_{OC} range was expanded to around 2.3 V. Furthermore, balanced and enhanced sub cell photocurrent densities were achieved by introducing n-doped μc-SiO_x:H layers for the top and bottom cells and a thicker n-type μc-SiO_x:H intermediate reflecting (IR) layer after the a-Si:H middle cell.[27,35,36] The latter ensures that more short wavelength light is reflected back into the two (top and middle) a-Si:H sub cells. Similar to the a-Si:H/μc-Si:H/μc-Si:H, this triple cell type used the same wide band gap a-Si:H top cell absorber layer. For the middle cell an a-Si:H absorber layer with lower band gap (1.91 eV ± 25 meV) was applied. We compared three different a-Si:H/a-Si:H/μc-Si:H devices (referred to as T5-T7):

- a reference solar cell prepared without μc-SiO_x:H n- and IR layers ("T5"),
- a cell with μc-SiO_x:H n- and IR layers ("T6"), and
- the same cell as T6, but with adapted sub cell thicknesses such that a balanced maximum current level is provided by each sub cells ("T7").

The experimental data of the triple junction cells, in terms of QE measured photocurrent densities of each individual sub cell, layer preparation (including layer thicknesses) and PV parameters are presented in Table 3.

Again, the J_{SC} values are higher compared to the J_{QE} values measured from the QE measurements because an anti-reflection foil was used for the *J–V* measurement. The integration of μc-SiO_x:H n-layers and IR layers significantly enhanced J_{SC} from 7.8 mA cm^{-2} (cell T5) to 8.3 mA cm^{-2} (cell T6), mainly due to the increase of the middle cell photocurrent density from 6.8 to 7.1 mA cm^{-2}. The current matched cell T7 provided the highest J_{SC} value of 8.6 mA cm^{-2} and a V_{OC} of 2279 mV. This shows that our approach results in an increase in 0.8 mA cm^{-2} and 10 mV relative to cell T5. The good current-matching for cell T7 also results in the slightly decreased fill factor. Overall an efficiency of 13.6% was obtained along with a V_{MPP} of 1851 mV with J_{MPP} of 7.1 mA cm^{-2}. Accordingly, in PV-EC device configuration, overpotential losses up to 600 mV (1.85–1.23 V), which is in the range of state-of-the-art precious metal catalyst materials for the HER and OER,[38,39] are tolerable to operate the device near its maximum power point. The application of the multijunction solar cells in integrated water splitting device will be discussed in Section 3.2. The quantum efficiency measurement of cell T7 is shown in Fig. 4.

A3. a-Si:H/a-Si:H/μc-Si:H/μc-Si:H quadruple junction solar cells. To increase the flexibility in choosing catalyst materials for water splitting, *e.g.* catalytically less active non-precious metals, a large excess voltage (>600 mV) is necessary. Open-circuit voltages of 2.8 V are feasible and were recently shown for quadruple cells.[40–42] In contrast to intrinsic a-SiO_x:H used as top cell absorber layer[41] or a-SiGe:H used as middle cell absorber material,[40] we applied the aforementioned wide band gap intrinsic a-Si:H material as top cell and the low band gap a-Si:H material as middle cell absorber layers. We used μc-SiO_x:H n-layers and integrated an IR layer between the middle a-Si:H and the first μc-Si:H sub cell. In order to match the sub cells in terms of the highest possible photocurrent, the thicknesses of each cell were systematically adjusted. The highest

Table 3 Overview of all relevant photocurrent densities (for each individual sub cell), layer preparation and PV parameters (V_{OC}, J_{SC}, FF, η) of a-Si:H/a-Si:H/μc-Si:H devices

Cell no.	μc-SiO_x:H ⟨n1⟩, IR, and ⟨n3⟩	$J_{QE,top}$ [mA cm^{-2}] (i-layer thickness [nm])	$J_{QE,mid}$ [mA cm^{-2}] (i-layer thickness [nm])	$J_{QE,bot}$ [mA cm^{-2}] (i-layer thickness [nm])	V_{OC} [mV]	J_{SC} [mA cm^{-2}]	FF [%]	V_{MPP} [mV]	J_{MPP} [mA cm^{-2}]	η [%]
T5	W/o	7.3 (80)	6.8 (400)	7.4 (1200)	2269	7.8	72.3	1859	6.9	12.8
T6	With	7.4 (80)	7.1 (400)	7.4 (1200)	2272	8.3	71.2	1860	7.1	13.4
T7	With (matched)	7.6 (90)	7.3 (700)	7.6 (1800)	2279	8.6	69.2	1851	7.4	13.6

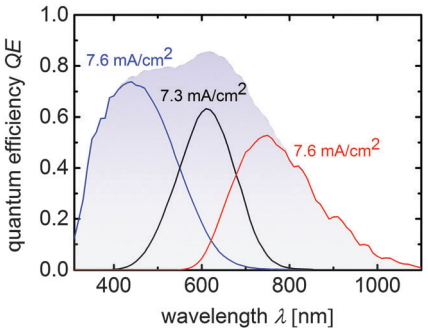

Fig. 4 Quantum efficiency curves of a a-Si:H/a-Si:H/μc-Si:H triple junction device corresponding to cell T7 from Table 3. Sub cell current densities calculated from the QE-curves are placed near the related measurements. The blue shaded area displays the total QE of the triple junction solar cell.

efficiency of 13.2% (V_{OC} = 2.802 V, J_{SC} = 6.8 mA cm^{-2}, and FF = 69.5%) was obtained for the a-Si:H/a-Si:H/μc-Si:H/μc-Si:H quadruple cell with the respective intrinsic absorber layer thicknesses: a-Si:H top cell absorber: 80 nm, a-Si:H middle cell absorber: 400 nm, μc-Si:H middle cell absorber: 1500 nm, and μc-Si:H bottom cell absorber: 2500 nm. Fig. 5 displays the spectral response of the quadruple cell with the highest efficiency.

In terms of water splitting, the high V_{MPP} of around 2278 mV (J_{MPP} = 5.8 mA cm^{-2}) provides over 1 V of excess voltage and thus offers a lot of freedom in the choice of the catalyst material, which will be discussed in the following section.

Overall, the presented photovoltaic development deviates from prevalent routes, as we focused on high adjustable output voltages rather than on record electrical conversion efficiencies. Nevertheless, the conversion efficiencies of the triple and quadruple junction solar cells presented in this study are very close to the highest efficiencies reported for solar cells made of thin film silicon.[43] Fig. 6 summarizes the multijunction solar cell development and presents the *J–V* measurements of the best developed triple (cell T4 and T7 from Tables 2 and 3) and quadruple junction solar cells along with the V_{OC} (2.0 V to 2.8 V) and V_{MPP} (1.6 V to 2.3 V) range.

In real photoelectrochemical systems however, overpotential losses cause that the operation point (theoretically at 1.23 V,

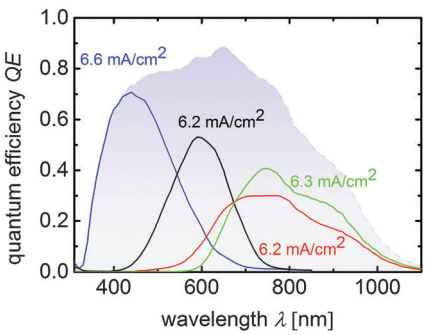

Fig. 5 Quantum efficiency curves of the a-Si:H/a-Si:H/μc-Si:H/μc-Si:H quadruple junction solar cell. Sub cell current densities calculated from the QE-curves are placed near the related measurements and the total QE is displayed by the blue shaded area.

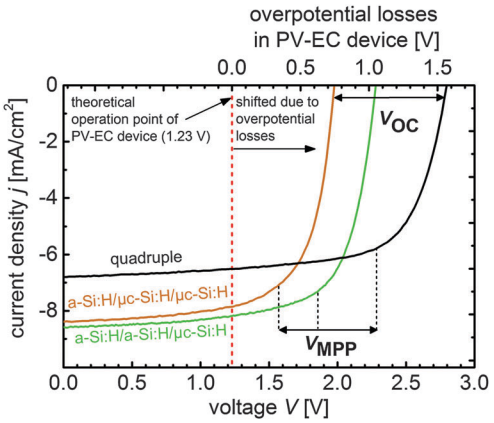

Fig. 6 Current voltage curves of the developed triple, and quadruple junction solar cells based on a-Si:H and μc-Si:H. The achievable V_{OC} (2.0 V to 2.8 V) and V_{MPP} (1.6 V to 2.3 V) ranges are indicated, respectively. The *J–V* curves of the triple and quadruple junction solar cells are linked with the theoretical operation point of a PV-EC device at 1.23 V (red dashed vertical line, without overpotential losses). In real PV-EC devices this operation point is shifted due to overpotential losses, which are plotted on the upper *x*-axis.

red vertical line in Fig. 6) is shifted towards more positive bias, as implied in Fig. 6. Assuming that all PV parameters of the solar cells remain unchanged when they are integrated in a PV-EC device, Fig. 6 allows to illustratively predict the performance of PV-EC devices based on our developed solar cells. The operation photocurrent density of a PV-EC device can be read at the crossing point of the solar cell *J–V* with the operation point line at the respective overpotential from the upper *x*-axis. As can be deduced from Fig. 6, the a-Si:H/a-Si:H/μc-Si:H triple junction could provide a maximum operation photocurrent density of 8.2 mA cm^{-2} when the PV-EC device would operate ideally, *i.e.* without any overpotential losses. When considering losses, the excess voltages become beneficial, as will be discussed in the following. Notwithstanding this, based on the presented photovoltaic results it is already possible to derive the practical performance limits of the state-of-the-art thin film silicon technology for water splitting applications.

B. Photovoltaic-biased electrosynthetic cells

B1. Calculation of solar-to-hydrogen efficiency. During operation the two electrodes (photocathode and anode) of the PV-EC device are shorted. The photocurrent density j_{op} at 0 V applied voltage can be used to estimate the STH efficiency of the PV-EC device using the following equation:[44]

$$\eta_{STH} = \frac{\text{power out}}{\text{power in}} = \frac{\Delta E \times j_{op}}{\text{total integrated power input density}} \quad (1)$$

ΔE = 1.23 V is the thermodynamic potential required for water electrolysis at 25 °C, j_{op} is the operating photocurrent density when no bias is applied, and the input power is the incident light intensity. Several different methodologies have been proposed in literature to evaluate the STH efficiencies of water splitting devices.[44–47] One well-established method is described

by eqn (1). This calculation underlies the assumption that the measured photocurrent corresponds to the molecular hydrogen generation *via* proton reduction (100% faradaic efficiency). The evaluation described above provides a consistent method for the comparison of the performance between various solar fuel production systems. The assumption of a faradaic efficiency of 100% for the system under study was confirmed by a volumetric measurement of the evolved gases (see Fig. S1 and S2, in the ESI†).

B2. Comparison of PV-EC devices based on triple and quadruple junction solar cells. Fig. 7 depicts the *J*–*V* measurements in two-electrode configuration of the real PV-EC devices based on the multijunction solar cells developed in section A and measured in 0.1 M KOH. Apparently, the shape of the curves is different from the pure solar cell *J*–*V* presented in Fig. 6. In particular the FF and V_{OC} are reduced, mainly because of the electrolyte resistance and the overpotential losses at the electrode surfaces (Pt and RuO_2), respectively. The saturation photocurrent is slightly reduced compared with the pure *J*–*V* measurement on the solar cells, because for the PV-EC measurements no anti-reflection foil was used. However, light absorption and physics of the photogenerated charge carrier separation within the solar cell remain unaffected when used as photocathode in the PV-EC device.

Above all, the measurements show that the highest photocurrent at 0 V applied bias is provided by the a-Si:H/a-Si:H/μc-Si:H based PV-EC device. The device operates near its MPP at 7.1 mA cm^{-2}, which, according to eqn (1), corresponds to a STH efficiency of 8.7% in 0.1 M KOH. For the a-Si:H/μc-Si:H/μc-Si:H based device further improvements in the fill factor of the solar cell (cell T4) have to be made in order to reach the MPP photocurrent in the short-circuit condition, and thus, achieve a higher STH efficiency. The operation point of the quadruple junction device lies at 6.2 mA cm^{-2}. Albeit the corresponding estimated 7.6% STH efficiency is lower compared to the a-Si:H/a-Si:H/μc-Si:H device for the respective catalysts, the quadruple junction device operates in a relatively flat region of the *J*–*V* curve (current plateau region). Hence, this device provides a certain excess voltage, which offers a higher flexibility in choosing other non-precious catalyst materials, as will be discussed in the following section. The experimental data of the three PV-EC devices are summarized in Table 4.

Table 4 Overview of the relevant parameters for the triple and quadruple based PV-EC devices using 0.1 M KOH as electrolyte, Pt as HER catalyst, and RuO_2 as OER catalyst. STH efficiencies are calculated based on the assumption of 100% faradaic efficiency

Photocathode	j_{op} [mA cm^{-2}]	η_{STH} [%]
a-Si:H/μc-Si:H/μc-Si:H	4.8	5.9
a-Si:H/a-Si:H/μc-Si:H	7.1	8.7
Quadruple	6.2	7.6

B3. Pt and Ni as HER catalysts. From Fig. 7, it can be deduced that for an approx. 200 mV increase in overpotential losses the quadruple based device would exhibit a higher STH efficiency than its a-Si:H/a-Si:H/μc-Si:H triple junction counterpart. To validate this result, we deposited Ni, instead of Pt on top of the quadruple and triple junction solar cell. Ni is catalytically less active than Pt, but as a non-precious and earth-abundant catalyst material it is alluring due to its cost-effectiveness.[48]

In Fig. 8, the *J*–*V* measurements of the triple and quadruple junction based PV-EC devices with Pt and Ni layers as HER catalysts, respectively are compared.

As expected, the operation photocurrent density j_{op} for the Ni-coated triple and quadruple devices is lower compared to the platinized devices. But the a-Si:H/a-Si:H/μc-Si:H based device shows a significant decrease in j_{op} from 7.1 to 6.1 mA cm^{-2}, while the quadruple based device only loses 0.1 mA cm^{-2} by using a Ni catalyst layer instead of Pt and still operates in the current plateau region. Both Ni-coated devices exhibit nearly the same estimated STH efficiency of 7.5% in 0.1 M KOH. However, the operation point of the triple junction based device lies in the steep slope of its *J*–*V* characteristics, where a slight

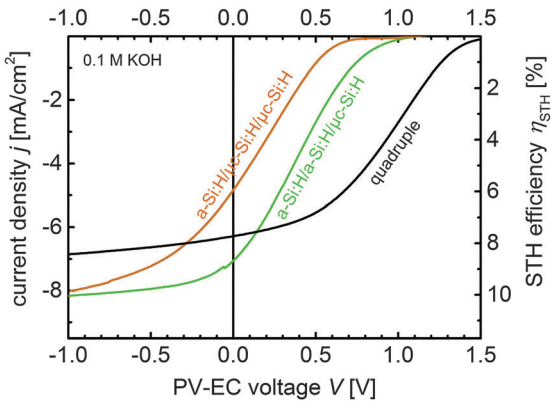

Fig. 7 *J*–*V* measurements of PV-EC devices based on thin film silicon multijunction photocathodes with a 150 nm thick Pt layer as HER catalyst and a RuO_2 counter electrode for the OER reaction. The measurements are conducted in 0.1 M KOH at 50 mV s^{-1}.

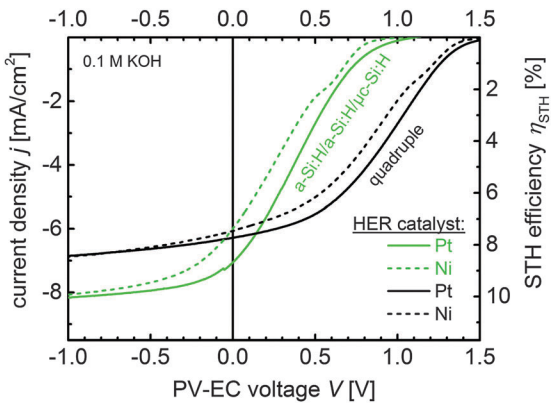

Fig. 8 *J*–*V* measurements of PV-EC devices based on a-Si:H/a-Si:H/μc-Si:H triple and quadruple junction photocathodes with RuO_2 counter electrode for the OER reaction. For the HER reaction 150 nm of Ni (dotted curves) and Pt (solid curves) were deposited on top of the solar cells, respectively. The measurements were conducted in 0.1 M KOH at 50 mV s^{-1}.

deterioration of the device parameters, due to photocorrosion during long-term operation for instance, can significantly deteriorate the STH efficiency. The operation point of the quadruple based device on the other hand lies in the plateau of its *J–V* characteristics, and thus, is less sensitive to photovoltage or fill factor variations.

B4. Electrolyte concentration. The effect of the KOH electrolyte concentration on the stability and performance of the triple (a-Si:H/a-Si:H/μc-Si:H) and quadruple junction based PV-EC devices are shown in Fig. 9(a) and (b), respectively. Fig. 9(a) displays the photocurrent density at 0 V applied bias monitored over a prolonged period of time for the quadruple junction based device with a Ni HER catalyst and for the a-Si:H/a-Si:H/μc-Si:H based device with a Pt HER catalyst in 0.1 M and 1 M KOH, respectively.

In 0.1 M KOH a stable photocurrent of approx. 6.1 mA cm^{-2} and 7.0 mA cm^{-2}, respectively, was measured for both PV-EC devices over the course of 4 hours (approx. 15 000 s). The periodical fluctuations in the photocurrent densities are caused by repetitive accumulation and detachment of H_2 bubbles at the photocathode surface. The measurements in 1 M KOH revealed that both devices did not operate longer than 1000 s. This result shows that a relatively small change in the pH value from approx. 13 to 14 has a significant effect on the stability of the PV-EC devices. In particular, pitting corrosion and delamination of the stacked metal layers at the solar cell-electrolyte interface prevented longer operation times. Here, adapted PV-EC device designs for robust water splitting operations need to be considered.[31]

Notwithstanding this, in the case of the triple junction based device an increase of 0.7 mA cm^{-2} in the operation photocurrent density j_{op} to 7.7 mA cm^{-2} is observed when 1 M KOH is used as electrolyte solution instead of 0.1 M KOH. From Fig. 9(b) it becomes apparent that this increase is caused by an improvement of the fill factor in the *J–V* curves of the triple junction based PV-EC devices. In fact, an increase in the electrolyte concentration reduces the series resistance of the complete PV-EC device, which leads to an improved fill factor. The effects of electrolyte resistance and other factors on the performance of PV-EC devices were investigated in more detail by modeling in a previous study.[12] According to eqn (1) an impressive STH efficiency of 9.5% can be estimated from the j_{op} of 7.7 mA cm^{-2} for the triple based PV-EC device with Pt as HER and RuO_2 as OER catalyst. Please note that the solar-to-hydrogen efficiencies calculated *via* eqn (1) represent an upper limit for the η_{STH} due to the assumption of unity faradaic efficiency.

Referring to a recently published overview of demonstrated STH conversion efficiencies,[11] this is the highest reported STH efficiency for an integrated monolithic thin film silicon based photoelectrochemical device. STH efficiencies over 10% would become feasible by using anti-reflection foils to enhance the saturation photocurrents of the a-Si:H/a-Si:H/μc-Si:H solar cell in the PV-EC device configuration by around 0.4 mA cm^{-2} from 8.2 to 8.6 mA cm^{-2} (see Fig. 6). However, the issue of photocorrosion, particularly present for electrolyte concentrations of or above 1 M, need to be solved at the same time. In this regard, the excess voltage provided by the quadruple junction based device offers an additional advantage. As apparent from Fig. 9(a) and (b), the increase in electrolyte concentration does not affect the operation photocurrent density of the device, which exhibits a j_{op} of 6.1 mA cm^{-2} for the *J–V* measurements conducted 0.1 M and 1 M KOH, respectively. This result can be understood, because the device operates in the current plateau, where an improved fill factor does not improve the current density (see Fig. 9(b)). This overall shows that quadruple junction solar cells not only promote the usage of cheaper catalyst materials, but also allow for the operation in low-concentrated electrolytes without impairing the device efficiency, and thus, for an increased long-term stability of the device and the catalysts.

In total, the presented PV-EC device concept in combination with the broad range of tunable photovoltages offers an important toolbox for the investigation of related research challenges, including catalyst development,[49] robust surface coating designs,[30] or integrated device architectures.[50]

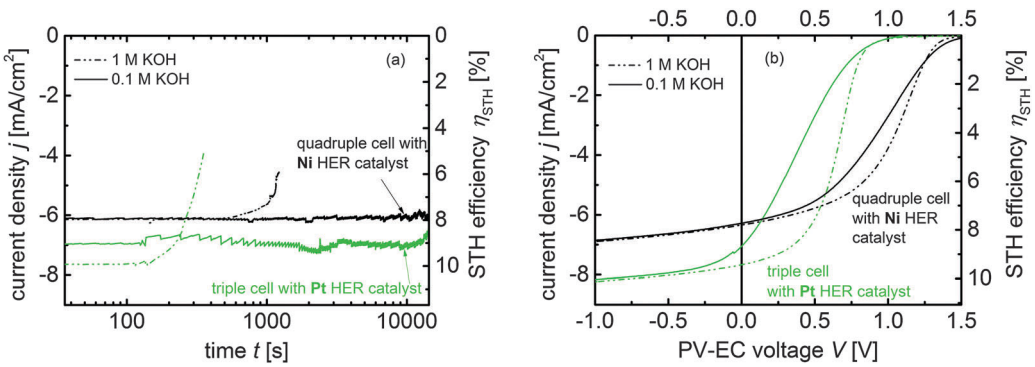

Fig. 9 (a) Chronoamperometric stability measurement monitoring the long-term stability of the a-Si:H/a-Si:H/μc-Si:H and the quadruple junction based PV-EC devices with Pt and Ni catalyst layers, respectively, at 0 V applied bias on a logarithmic time scale. The measurements were conducted in 0.1 M (solid curves) and in 1 M KOH (dotted curves) under AM 1.5 illumination (100 mW cm^{-2}). As a counter electrode for the OER reaction RuO_2 was used. (b) *J–V* measurements of the triple and quadruple junction based PV-EC devices in 0.1 M (solid curves) and 1 M KOH (dotted curves). The measurements were conducted at a scan rate of 50 mV s^{-1}.

IV. Summary

The present study outlined the important steps towards designing highly efficient semiconductor structures and the presented results provide evidence that stable STH efficiencies over 10% are within the reach of thin film silicon based devices. We presented in detail the development of triple and quadruple junction solar cells based on a-Si:H and μc-Si:H and demonstrated their applicability for efficient solar water splitting. The series-connected multijunction cell configurations provided a wide range of achievable V_{OC} (2.0 V to 2.8 V) and V_{MPP} (1.6 V to 2.3 V) voltages. Additionally, we were able to systematically tune the V_{OC} of the solar cells within a smaller voltage range (~50 mV) without impairing the device efficiency, a feature which is highly important to compensate the losses occurring in photoelectrochemical applications. Overall, by carefully adjusting the photocurrents of the sub cells we achieved PV efficiencies of 13.6% for triple and 13.2% for quadruple junction solar cells. The application in PV-EC devices showed that the a-Si:H/a-Si:H/μc-Si:H based PV-EC device with Pt as hydrogen evolution catalyst and RuO_2 as oxygen evolution catalyst exhibited 7.7 mA cm^{-2} at 0 V applied bias, which corresponds to a solar-to-hydrogen efficiency of 9.5% (assuming a 100% faradaic efficiency). The PV-EC device based on a quadruple junction cell (a-Si:H/a-Si:H/μc-Si:H/μc-Si:H) exhibited enough excess voltage to substitute Pt as precious metal catalyst by a more abundant material, such as Ni, and to work in low-concentrated electrolyte solutions without impairing the solar-to-hydrogen efficiency. With Ni as HER catalyst, this device provided 6.1 mA cm^{-2} at 0 V applied bias over the course of 4 hours.

Conflict of interest

The authors declare no competing financial interests.

Acknowledgements

We thank U. Gerhards, L. Petter, W. Reetz, and H. Siekmann, for their contributions to this work. The research is partly financially supported by the Deutsche Forschungsgemeinschaft (DFG) Priority Programme 1613 (SPP 1613): Regeneratively produced fuels by light-driven water splitting: Investigation of involved elementary processes and perspectives of technologic implementation, and by the German Bundesministerium für Bildung und Forschung (BMBF) in the network project: Sustainable Hydrogen (FKZ 03X3581A and FKZ 03X3581B). J. Ziegler, F. Yang, B. Kaiser, and W. Jaegermann acknowledge partial financial support by the DFG Excellence Graduate School of Energy Science and Engineering (GSC 1070).

References

1 T. R. Cook, D. K. Dogutan, S. Y. Reece, Y. Surendranath, T. S. Teets and D. G. Nocera, *Chem. Rev.*, 2010, **110**, 6474–6502.
2 C. A. Grimes, O. K. Varghese and S. Ranjan, *Light, water, hydrogen: the solar generation of hydrogen by water photoelectrolysis*, Springer, New York, 2008.
3 A. J. Nozik and R. Memming, *J. Phys. Chem.*, 1996, **100**, 13061–13078.
4 E. Miller, *White Papers on Materials for Photoelectrochemical Water Splitting*, DOE PEC Working Group, 2013.
5 Z. Li, W. Luo, M. Zhang, J. Feng and Z. Zou, *Energy Environ. Sci.*, 2013, **6**, 347–370.
6 R. Memming, *Semiconductor Electrochemistry*, Wiley VCH, 2002.
7 A. C. Nielander, M. R. Shaner, K. M. Papadantonakis, S. A. Francis and N. S. Lewis, *Energy Environ. Sci.*, 2015, **8**, 16–25.
8 B. Parkinson, *Acc. Chem. Res.*, 1984, **17**, 431–437.
9 F. Urbain, K. Wilken, V. Smirnov, O. Astakhov, A. Lambertz, J.-P. Becker, U. Rau, J. Ziegler, B. Kaiser, W. Jaegermann and F. Finger, *Int. J. Photoenergy*, 2014, **2014**, 249317.
10 F. F. Abdi, L. Han, A. H. M. Smets, M. Zeman, B. Dam and R. van de Krol, *Nat. Commun.*, 2013, **4**, 2195.
11 J. W. Ager, M. R. Shaner, K. A. Walczak, I. D. Sharp and S. Ardo, *Energy Environ. Sci.*, 2015, **8**, 2811–2824.
12 F. Urbain, V. Smirnov, J.-P. Becker, U. Rau, J. Ziegler, B. Kaiser, W. Jaegermann and F. Finger, *Sol. Energy Mater. Sol. Cells*, 2015, **140**, 275–280.
13 T. J. Mills, F. Lin and S. W. Boettcher, *Phys. Rev. Lett.*, 2014, **112**, 148304.
14 Z. Huang, J. R. McKone, C. Xiang, R. L. Grimm, E. L. Warren, J. M. Spurgeon, H.-J. Lewerenz, B. S. Brunschwig and N. S. Lewis, *Int. J. Hydrogen Energy*, 2014, **39**, 16220–16227.
15 A. E. Delahoy, S. C. Gau, O. J. Murphy, M. Kapur and J. O'M. Bockris, *Int. J. Hydrogen Energy*, 1985, **10**, 113–116.
16 S. Y. Reece, J. A. Hamel, K. Sung, T. D. Jarvi, A. J. Esswein, J. J. H. Pijpers and D. G. Nocera, *Science*, 2003, **334**, 645–648.
17 V. Cristino, S. Berardi, S. Caramori, R. Argazzi, S. Carli, L. Meda, A. Tacca and C. A. Bignozzi, *Phys. Chem. Chem. Phys.*, 2013, **15**, 13083–13092.
18 L. Han, I. A. Digdaya, T. W. F. Buijs, F. F. Abdi, Z. Huang, R. Lui, B. Dam, M. Zeman, W. A. Smith and A. H. M. Smets, *J. Mater. Chem. A*, 2015, **3**, 4155–4162.
19 R. E. Rocheleau, E. L. Miller and A. Misra, *Energy Fuels*, 1998, **12**, 3–10.
20 O. Khaselev, A. Bansal and J. A. Turner, *Int. J. Hydrogen Energy*, 2001, **26**, 127–132.
21 K. Fujii, S. Nakamura, M. Sugiyama, K. Watanabe, B. Bagheri and Y. Nakano, *Int. J. Hydrogen Energy*, 2013, **38**, 14424–14432.
22 T. J. Jacobsson, V. Fjällström, M. Sahlberg, M. Edoff and T. Edvinsson, *Energy Environ. Sci.*, 2013, **6**, 3676–3683.
23 C. R. Cox, J. Z. Lee, D. G. Nocera and T. Buonassisi, *Proc. Natl. Acad. Sci. U. S. A.*, 2014, **111**, 14057–14061.
24 J. Luo, J.-H. Im, M. T. Mayer, M. Schreier, M. Khaja Nazeeruddin, N.-G. Park, S. D. Tilley, H. Jin Fan and M. Grätzel, *Science*, 2014, **345**, 1593–1596.
25 F. Finger, R. Carius, T. Dylla, S. Klein, S. Okur and M. Günes, *IEE Proc., Part I: Solid-State Electron Devices*, 2003, **150**, 300–308.

26 F. Urbain, V. Smirnov, J.-P. Becker, U. Rau, J. Ziegler, B. Kaiser, W. Jaegermann and F. Finger, *J. Mater. Res.*, 2014, **29**, 2605–2614.
27 A. Lambertz, V. Smirnov, T. Merdzhanova, K. Ding, S. Haas, G. Jost, R. E. I. Schropp, F. Finger and U. Rau, *Sol. Energy Mater. Sol. Cells*, 2013, **119**, 134–143.
28 S. Hu, M. R. Shaner, J. A. Beardslee, M. Lichterman, B. S. Brunschwig and N. S. Lewis, *Science*, 2014, **344**, 1005–1009.
29 M. J. Kenney, M. Gong, Y. Li, J. Z. Wu, J. Feng, M. Lanza and H. Dai, *Science*, 2014, **342**, 836–840.
30 B. Mei, B. Seger, T. Pedersen, M. Malizia, O. Hansen, I. Chorkendorff and P. C. K. Vesborg, *J. Phys. Chem. Lett.*, 2014, **5**, 1948–1952.
31 N. A. Kelly and T. L. Gibson, *Int. J. Hydrogen Energy*, 2006, **31**, 1658–1673.
32 W. Böttler, V. Smirnov, J. Hüpkes and F. Finger, *Phys. Status Solidi A*, 2012, **209**, 1144–1149.
33 C. Ulbrich, A. Gerber, K. Hermans, A. Lambert and U. Rau, *Prog. Photovoltaics*, 2013, **21**, 1672–1681.
34 G. Hodes, *J. Phys. Chem. Lett.*, 2012, **3**, 1208–1213.
35 V. Smirnov, A. Lambertz, S. Tillmanns and F. Finger, *Can. J. Phys.*, 2014, **92**, 932–935.
36 S. Kirner, S. Calnan, O. Gabriel, S. Neubert, M. Zelt, B. Stannowski, B. Rech and R. Schlatmann, *Phys. Status Solidi C*, 2012, **9**, 2145–2148.
37 S. Hänni, M. Boccard, G. Bugnon, M. Despeisse, J.-W. Schüttauf, F.-J. Haug, F. Meillaud and C. Ballif, *Phys. Status Solidi A*, 2015, **212**, 840–845.
38 L. C. Seitz, Z. Chen, A. J. Forman, B. A. Pinaud, J. D. Benck and T. F. Jaramillo, *ChemSusChem*, 2014, **7**, 1372–1385.
39 C. C. L. McCrory, S. Jung, J. C. Peters and T. F. Jaramillo, *J. Am. Chem. Soc.*, 2013, **135**, 16977–16987.
40 J.-W. Schüttauf, B. Niesen, L. Löfgren, M. Bonnet-Eymard, M. Stuckelberger, S. Hänni, M. Boccard, G. Bugnon, M. Despeisse, F.-J. Haug, F. Meillaud and C. Ballif, *Sol. Energy Mater. Sol. Cells*, 2015, **133**, 163–169.
41 F. T. Si, D. Yun Kim, R. Santbergen, H. Tan, R. A. C. M. M. van Swaaij, A. H. M. Smets, O. Isabella and M. Zeman, *Appl. Phys. Lett.*, 2014, **105**, 063902.
42 S. Kirner, S. Neubert, C. Schultz, O. Gabriel, B. Stannowski, B. Rech and R. Schlatmann, *Jpn. J. Appl. Phys.*, 2015, **54**, 08KB03.
43 M. Green, K. Emery, Y. Hishikawa, W. Warta and E. D. Dunlop, *Prog. Photovoltaics*, 2015, **23**, 1–9.
44 Z. Chen, T. F. Jaramillo, T. G. Deutsch, A. Kleiman-Shwarsctein, A. J. Forman, N. Gaillard, R. Garland, K. Takanabe, K. Heske, M. Sunkara, E. W. McFarland, K. Domen, E. Miller, J. A. Turner and H. N. Dinh, *J. Mater. Res.*, 2010, **25**, 3–16.
45 M. G. Walter, E. L. Warren, J. R. McKone, S. W. Boettcher, Q. Mi, E. A. Santori and N. S. Lewis, *Chem. Rev.*, 2010, **110**, 6446–6473.
46 Z. Chen, H. N. Dinh and E. Miller, *Photoelectrochemical Water Splitting*, Springer, New York, 2013.
47 R. H. Coridan, A. C. Nielander, S. A. Francis, M. T. McDowell, V. Dix, S. M. Chatman and N. S. Lewis, *Energy Environ. Sci.*, 2015, **8**, 2886–2901.
48 J. R. McKone, E. L. Warren, M. J. Bierman, S. W. Boettcher, B. S. Brunschwig, N. S. Lewis and H. B. Gray, *Energy Environ. Sci.*, 2011, **4**, 3573–3583.
49 K. Maeda and K. Domen, *J. Phys. Chem. Lett.*, 2010, **1**, 2655–2661.
50 B. Seger, I. E. Castelli, P. C. K. Vesborg, K. W. Jacobsen, O. Hansen and I. Chorkendorff, *Energy Environ. Sci.*, 2014, **7**, 2397–2413.

